Journal of the Optical Society of America A
OPTICS, IMAGE SCIENCE, AND VISION

Guided Bloch surface wave resonance for biosensor designs

Xiu-Bao Kang,[1,*] Lan-Jun Liu,[1] Hai Lu,[2] Hai-Dong Li,[1] and Zhi-Guo Wang[3]

[1]School of Science, Henan Institute of Engineering, Zhengzhou, Henan 451191, China
[2]College of Physics and Electronic Engineering, Henan Normal University, Xinxiang 453007, China
[3]School of Physics Science and Engineering, Tongji University, Shanghai 200092, China
*Corresponding author: kang@haue.edu.cn

Received 4 January 2016; revised 1 April 2016; accepted 2 April 2016; posted 4 April 2016 (Doc. ID 256655); published 29 April 2016

A guided Bloch surface wave resonance (GBR) configuration is introduced for label-free biosensing. The GBR is realized by coupling the first-order diffraction of a subwavelength grating with the Bloch surface wave at the interface between a 1D photonic crystal slab and bio-solution. In addition to sustaining the Bloch surface mode, the photonic crystal provides the design freedom of simultaneously increasing the quality and decreasing the sideband transmissions of the resonance spectrum. The low sideband and high-quality features along with the large sensitivity rising from the strong overlap between the Bloch surface mode and the bio-solution make the GBR suitable for the design of biosensors. Biosensors with a high figure of merit are realized by the compact configurations. © 2016 Optical Society of America

OCIS codes: (050.0050) Diffraction and gratings; (280.4788) Optical sensing and sensors; (260.5740) Resonance; (240.6690) Surface waves.

http://dx.doi.org/10.1364/JOSAA.33.000997

1. INTRODUCTION

Owing to the ever-increasing demands for label-free and cost-free biosensing, many research interests have been focused on optical biosensor designs [1]. To distinguish the generally small modulations of optical parameter(s) caused by the concentration of the bio-molecules [2–5], various kinds of resonances such as surface plasmon polaritons (SPPs) [6–9], cavity [3,10], guided-mode resonance (GMR) [11–13], and Bloch surface wave (BSW) [2,5,14–20] resonances have been used in those designs. The steep scattering spectra and the enhanced light-matter interaction by the electromagnetic (EM) field localized near the resonance make the EM wave scattering from the devices more sensitive to changes in the bio-solution.

Current commercial optical biosensors rely on SPP, which occurs at the interface between metal and bio-solution [7,8]. As a kind of surface wave, the SPP mode is strongly localized near the interface. Because of the strong overlap between the resonant mode and the bio-solution and the fact that SPPs are excited at wavelengths where the metals offer strong dispersion, SPP sensors can achieve large sensitivities S (the sensitivity, defined as the resonance spectral shift over a perturbation in the refractive index of bio-solution). The surfaces of SPP biosensors are generally in the order of several hundred $\mathrm{nm\,RIU^{-1}}$ ($\Delta\lambda/\Delta n$) [21,22]. Unfortunately, accompanying the strong dispersion, absorption is inevitable in the metal components. The absorption leads to small quality factors for the SPP resonances. The small quality factors inevitably increase the ambiguity in detecting the shifts of the transmission peak, and the performance of the corresponding sensors will be reduced. The most widely adapted metric for the intrinsic spectrum resolving power of an optical sensor is the figure of merit $\mathrm{FOM} = S(\mathrm{nm}\cdot\mathrm{RIU}^{-1})/\Gamma(\mathrm{nm})$, where Γ is the FWHM of the resonance. In the SPP sensors design, the FOM is generally less than 100 [23–25]. As another kind of surface wave, BSW at the interface of 1D photonic crystals (PhCs) and bio-solutions has also been used in the design of biosensors. Due to the absence of the absorption in the general all-dielectric BSW configurations, the quality of a BSW resonance is generally higher than that of SPP resonances. By increasing the number of periods of the PhC, the quality factor of the BSW resonance can be made as high as or even go beyond the fabrication and detection limit of current technology. Furthermore, the BSW features more degrees of design freedom (the thicknesses, refractive indices of the composing dielectric layers). The BSW can be excited at any wavelength by both polarizations and can be well incorporated with porous [5,26] or fluorescence mechanisms [4] to achieve better performance for the corresponding biosensors.

Biosensor designs based on GMR have also been well studied [13,27,28]. Comparing with the BSW resonances, GMRs feature both higher-quality factors and more compact configurations [12]. In GMR biosensor designs, biomolecular solutions are generally localized inside or adjacent to the gratings. The

refractive index modulations of the bio-solution induced by the different concentration ratio of the biomolecules effectively shift the resonance of the guided mode, and thus the scattering from the structures. As the resonantly enhanced guided-mode generally decays rapidly in the substrate, the sensitivity of a GMR sensor is then limited by the small overlap between the resonant guided mode and the bio-solution. The sensitivities of biosensors relying on the GMRs are generally in the same order but smaller than that of SPP biosensors (e.g., 82.5 nm RIU^{-1} in single grating layer and $S = 189.1$ nm RIU^{-1} for the grating mono-layer configuration in [13]). Although a GMR is generally less sensitive to the refractive index modulations, the narrow spectral width of the resonance guarantees large FOM for the GMR sensors [27,28]. However, in the biosensor applications, the fragile feature of the gratings limits the application of the GMR sensors and the cleaning of the sensing region is not easy.

By combining the BSW and the GMR resonance, a guided BSW resonance (GBR) mechanism is studied for the biosensor designs in this paper. The GBR is realized by depositing sub-wavelength gratings on the surface of a Bragg mirror, which supports BSW on the other side. The grating is designed such that the normally incident EM wave can be coupled to the BSW by receiving a reciprocal lattice vector. The BSW resonance leads to enhancement of the coupling diffraction order, and thus the high-quality Fano resonance [29] in the scattering spectrum. Although only transverse-electric polarization near the working wavelength of $\lambda_0 \approx 650$ nm is studied, the GBR can also be excited in the transverse-magnetic case at any wavelength. The GBR configuration is shown to have the advantages of the GMR and the BSW resonance in the biosensor designs. The paper is organized as follows. In Section 2, the GBR biosensor configuration and the design principles of the GBR sensors are introduced. The performance of the GBR sensors is discussed in Section 3. In Section 4, the summary and conclusion are given.

2. BIOSENSOR BASED ON GUIDED BLOCH SURFACE WAVE RESONANCE

The schematic of a GBR biosensor is shown in Fig. 1. The structure is made by depositing a sub-wavelength grating on the one dimensional PhC with symmetric unit cells (HLH)

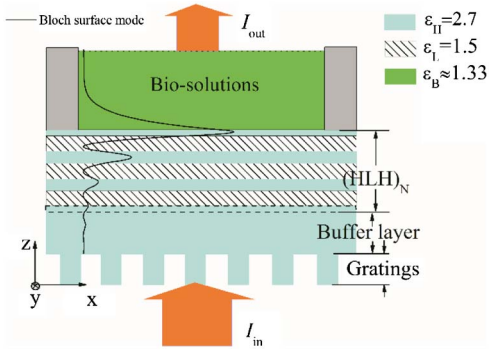

Fig. 1. Schematic of a guided Bloch surface wave resonance (GBR) biosensor. The structure is a combination of a few-period photonic crystal and subwavelength gratings. The solid line schematically shows the electric field distribution of the Bloch surface wave.

where the "H" and "L," respectively, represent dielectric components with the refractive indices being $n_H = 2.7$ and $n_L = 1.5$. The N ranging from 3 to 5 is the number of the periods of the PhCs. There is a buffer layer which is also made of high refractive index composites inserted between the Bragg mirror and the sub-wavelength grating. On the other side of the PhC, there is the probe range filled with thick bio-solution with the refractive index being $n_B \approx 1.33$. The probing EM wave impinges normally from the sub-wavelength grating side. The far field zeroth-order diffraction is then recorded and interrogated to distinguish changes in the concentration ratio of the bio-molecules.

It is well known that an EM wave propagates through a grating via the grating's eigenmodes which can be expanded as the superposition of low diffraction orders [30]. Generally, the eigenmode dominated by the zeroth-order diffraction is easier to be excited for the smaller tangential wave vector mismatch between the eigenmode and the incident EM wave. When one of the high-order diffractions (1st, 2nd…) experiences a resonance, the eigenmode dominated by this diffraction order will be enhanced accordingly. In the biosensor configuration shown in Fig. 1, the period of the grating is designed such that the normally incident EM wave can be coupled to BSW at the PhC–solution interface by receiving a single reciprocal wave vector. The resonance of the BSW then enhances the grating eigenmode dominated by the first-order diffraction. The zeroth-order diffraction can then pass through the grating via the grating's eigenmode dominated by the first-order diffraction and leaks through the Bragg mirror, which is a resonant path for the incident EM wave. The grating parameters are optimized to reach the resonant enhancement of the eigenmode dominated by the first-order diffraction inside the grating. The zeroth-order diffraction also penetrates the grating via gratings eigenmode dominated by the zeroth-order diffraction, which forms the nonresonant path for the zeroth-order diffraction. The interference between the zeroth-order diffraction, respectively, through these two paths leads to the Fano spectrum of the GBR structure. In the sensing process, the changes in the concentration ratio of the biomolecules in the substrate will modify the refractive index of the bio-solution. The resulting impedance variations then shift the resonance of the BSW and thus the Fano spectrum. The concentration ratio modulations can be measured by the shifts in the peak of the corresponding Fano spectrum. As both the probing and the detecting wave are normal to the PhC, no coupling equipment or angular spectrometer is needed, and thus the global sensor configuration is compact. The electric field distribution in the PhC-solution structure when GBR occurs is schematically shown. One can clearly find that there is strong field localization in the bio-solution. The overlap between the strong field localization of the BSW and the bio-solution guarantees large sensitivity for the GBR biosensors.

The performance of a biosensor is not determined only by the sensitivity of the resonance. When the HWFM of the resonance is decreased, the discrimination and thus the FOM of the biosensor can be increased. In the GBR sensor, two resonances are utilized to reach the strong transmission enhancement of the zeroth-order diffraction through the resonant

path (the BSW resonance at the PhC–solution interface and the resonance of the grating eigenmode dominated by the first-order diffraction). The hybridizing of these two resonances will undoubtedly lead to high-quality factors for the resonant path of the zeroth-order diffraction. Furthermore, suppressing the transmission neighboring the high-quality resonance may also improve the performance of the corresponding biosensors [15,28]. Although high-quality resonance with low sidebands can be realized with subwavelength gratings [31], the PhC adhering the subwavelength grating in the GBR configuration provides additional design freedoms for both the suppression of the sideband and the increase of the quality factor of the resonance.

In the GBR biosensor design, the grating period $\Lambda = 434$ nm is approximately 2/3 of the probing wavelength $\lambda_0 \approx 650$ nm. Such a period is designed to ensure that, in the low refractive index layer (L, $n_L = 1.5$), there is a near-zero normal wave vector component for the first-order diffraction:

$$k_L^1 = k_0\sqrt{n_L^2 - \left(\frac{\lambda}{\Lambda}\right)^2} \ll k_0. \tag{1}$$

By this small normal wave vector component, the phase delay of the first-order diffraction in the L layers changes slowly with the variation of d_L, where the phase delay

$$\Phi_L^1 = k_L^1 d_L. \tag{2}$$

The BSW and thus the eigenmode dominated by the first-order diffraction in the grating will be kept under sufficiently large modulations in d_L. At the same time, the normal wave vector component of the zeroth-order diffraction in the L layers is much larger:

$$k_L^0 = \frac{2\pi}{\lambda} \gg k_L^1. \tag{3}$$

The variations in d_L will effectively modulate the phase delay and thus the propagation of the zeroth-order diffraction in the PhC. As a result, the grating eigenmode dominated by the zeroth-order diffraction can well be modulated by the d_L. The low refractive index layer then provides the possibility of independently modulating the nonresonant, while keeping the resonant path of the zeroth-order diffraction. Thus, the Fano spectrum of the GBR can be conveniently controlled.

In the design of the PhCs, the Bloch wave expansion method [32] is employed. EM wave in the bandgap of the PhCs takes the form of two eigenmodes, the forward and backward decaying modes. The ratio between the tangential electric and magnetic field components of an eigenmode is the Bloch impedance for the corresponding eigenmode. When the Bloch impedance for the backward decaying eigenmode of the PhC matches the surface impedance of the decaying first-order diffraction in the bio-solution, there should be BSW at the PhC–solution interface. The surface impedance here is the ratio between the tangential components of, respectively, the electric and magnetic field of the first-order diffraction at the surface of the bio-solution. To reach the match of these two impedances, we first take a rough thickness for the low refractive index layer and interrogate the match of the two kinds of impedance. When $d_H = 38$ nm, the Bloch impedance and the surface impedance match each other, and there will then be BSW resonance at the interface. Then, we fix the d_H and search the d_L to ensure the zeroth-order diffraction also lies near the center of a PhC bandgap. As the normal wave vector component of the first-order diffraction in the low refractive index layer is very small, the Bloch impedance is insensitive to d_L, and thus the BSW is kept in the modification of the d_L. Further, to locate the incidence inside the bandgap, one does not require high precision for the layer thickness and $d_L = 100$ nm is used in this paper.

In Fig. 2(a), the dispersion of the PhC is given. The shaded region is the stop band of the PhC. The dotted and the dashed lines are, respectively, the light line of the bio-solution ($n_B = 1.33$) and the low refractive index layer ($n_L = 1.5$). The solid line is the dispersion curve for the BSW mode lying at the PhC–solution interface. By the properly designed grating period ($\Lambda = 434$ nm), the incident P_0 mode (normally impinging EM wave with the wavelength of 650 nm) is shifted to the mode $P_{1\,\mathrm{st}}$, which lies near the cross point between the dispersion curve for the BSW and the light line of the low refractive index dielectric, by receiving a reciprocal wave vector. The incident EM wave is then coupled to the BSW. There is then the GBR. As the refractive index of the bio-solution and that of the low refractive index layer have similar values ($n_B = 1.33$, $n_L = 1.5$), the $P_{1\,\mathrm{st}}$ mode lies very near to the light line of the solution. There is then a small extinction coefficient,

$$\kappa \approx k_0\sqrt{n_L^2 - n_B^2} \approx 0.694 k_0, \tag{4}$$

for the BSW mode in the solutions. By such a small κ, the BSW can well extend to the bio-solution (the strength of the EM field gets halved after propagating about 100 nm in the

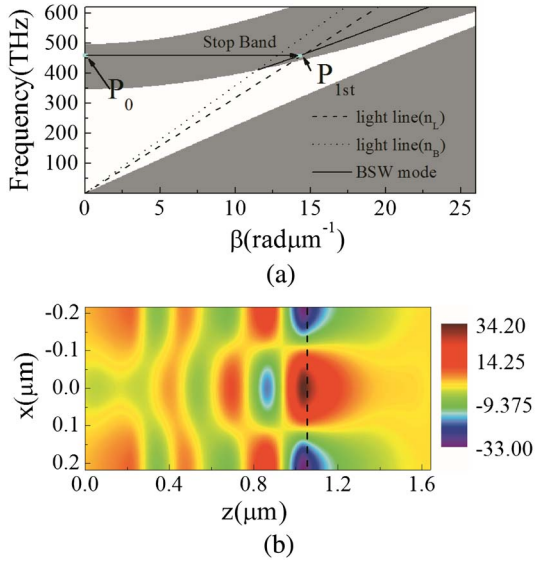

Fig. 2. (a) Dispersion of the PhCs with (LHL) unit-cell configuration. The shaded region shows the stop band. The solid line (without an arrowhead) is the dispersion curve of the BSW at the PhC–solution interface. The P_0 mode is the normally illuminating mode with the wavelength being 650 nm, and the $P_{1\,\mathrm{st}}$ mode is the first diffraction order. (b) Electric field inside the GBR structure under P_0 mode illumination. Thickness of the bio-solution is 600 nm. Dashed line indicates the interface between the PhC and the solution.

solutions). Comparing with the case of SPP sensor where the EM field decays fast inside the bio-solution for the large tangential wave vector component, the current sensor design can detect refractive index modulation much farther away from the devices. In Fig. 2(b), the electric field enhancement for the GBR sensor with the thickness of the bio-solution being 600 nm is given. The number of the periods of the PhC is 4. The thicknesses of the gratings and the buffer layer are, respectively, 200 and 320 nm. The filling factor of the gratings is $f = 0.4$. Scattering matrix method based on rigorous coupled wave analysis [33] is used here and in the following calculations. The dashed line in Fig. 2(b) indicates the PhC–solution interface and $z = 0$ is the grating side surface of the GBR sensor. One can clearly find that the electric field is strongly enhanced near the interface and the penetrating depth of the BSW is up to 100 nm inside the solutions. When the n_L gets closer to n_B, the BSW mode located near the light line of the low refractive index layer can penetrate deeper into the bio-solution, and the sensing ability of the sensor may be further increased.

Recently, BSW excited by Kretschmann scheme has been well studied for the design of biosensors [14–19]. Because the illuminations in those designs are nonpropagating in the substrate, absorption is necessary (otherwise, there should always be total reflection). When the BSW is excited, the EM field is strongly localized near the surface, and the resulting absorption enhancement leads to a dip in the reflection. By interrogating the reflection, the refractive index modulations are recorded. Sinibaldi *et al.* studied the influence of material losses on the performance of the BSW sensors [17]. As the BSW is mainly localized in the low refractive index layers of the PhC, the authors theoretically introduced an extinction ratio ranging from 0 to 1×10^{-3} to the refractive index of the corresponding layers. Loss in the GBR sensor may rise from the radiative loss caused by the surface roughness and the nonradiative absorption by imperfections inside the dielectric components [20]. Especially, as the EM wave is well localized near the PhC–solution interface and has a long lifetime, material losses in the bio-solution will greatly affect the transmission from the structure. To study the influence of loss, the transmission spectrum from the structure studied in Fig. 2(b) with and without considering the loss is given in Fig. 3. When considering loss, an imaginary part as large as 1×10^{-3} is added to the permittivity of the solution. One can find that the amplitude of the transmission and the quality of the resonance are suppressed when the loss is taken into consideration, while the position of the peak has not been affected. The result is consistent with that in the literature [14–19]. One should note that, because the first-order diffraction is set to the bandgap of the PhC, the background transmission near the GBR resonance peak is well suppressed. The peak is then still clearly distinguishable, even when the large material loss is considered. However, the material absorption of the dielectrics in the visible range can be made very low. At the same time, absorption is not essential in the GBR sensors design. We believe that the GBR sensor with much lower loss is within reach of current fabrication techniques and the influence of loss will be much weaker in realistic sensor processes. In the following, we only consider the lossless cases.

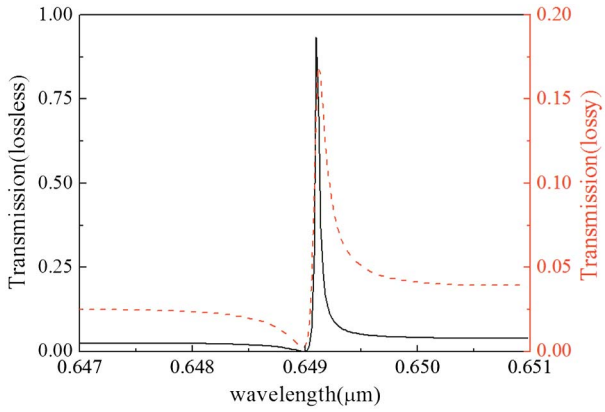

Fig. 3. Transmission spectrum of the structure studied in Fig. 2(b). Solid line is the case where all the components are lossless; red dashed line shows the lossy case when a 1×10^{-3} imaginary part is added to the permittivity of the bio-solution.

In the sensing applications, the thickness of the aqueous sample is generally not easy to be controlled. Fortunately, the exact thickness of the bio-solution does not affect much the transmission near the GBR. Although the zeroth-order diffraction is propagating in the substrate and used as the detecting signal, the location of the zeroth-order transmission peak is determined by the resonance of the BSW excited by the first-order diffraction. The evanescent feature of the BSW in the bio-solution proves that, when the solution is thick enough, thickness variations of the bio-solution layer have little effect on the BSW resonance. The Fano spectrum is then robust against variations in the thickness of the bio-solution layer. In Fig. 4, the transmission spectra from the GBR sensor configuration, with the thicknesses of the bio-solution being, respectively, 2.0, 2.1, 2.2, 2.3, 2.4, and 2.5 μm, are provided. The thickness and the filling factor of the gratings are, respectively, $d_G = 230$ nm and $f = 0.4$. One can find that, by the three-period PhC, the sideband of the transmission spectrum is well suppressed. The asymmetry spectrum with a sharp peak is just the result of the resonance of the BSW at the PhC–solution interface. Although, in the studied wavelength range, the phase delay of the zeroth-order diffraction in the 0.5 μm thickness

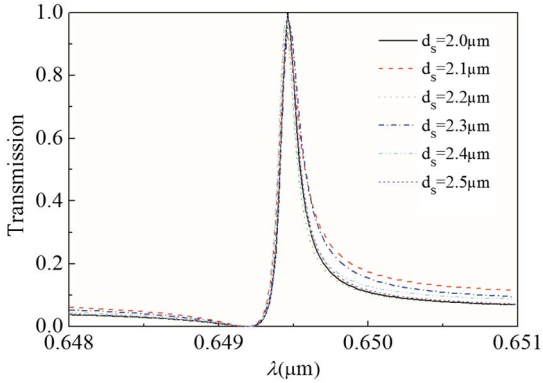

Fig. 4. GBR spectra with different bio-solution thicknesses. The dSs are, respectively, set as 2.0, 2.1, 2.2, 2.3, 2.4, and 2.5 μm.

variation experiences a roughly 2π shift, the shape and the location of the Fano spectra do not change much. The result is in good agreement with our former analysis. In the following, the thickness of the bio-solution layer is set as 2.4 μm.

3. SENSING BY GUIDED BLOCH SURFACE WAVE RESONANCE

Optical biosensors generally detect the small refractive index modulations caused by the concentration ratio variations of biomolecules. Figure 5 gives the shifts of the Fano spectra of GBR structures when the refractive index of the bio-solution is slightly changed. In Figs. 5(a)–5(c), the GBR structures, with the numbers of the PhC periods being, respectively, 3, 4, and 5, are studied. Although Bragg mirrors of so few periods cannot reflect much of incident wave, the transmissions surrounding the GBR Fano spectra are well-suppressed. The grating here also works as a high-quality reflector near the Fano resonance [29].

One can clearly find that, by using PhC with more periods, twofold benefits are reached. First, the sideband of the Fano transmission is further suppressed, which should owe to the fact that Bragg mirrors with more periods can reflect more of the zeroth-order diffraction. The lower sidebands undoubtedly make distinguishing the resonant peak easier and can well increase the detection limits of the GBR biosensors. Second, use of PhC with more periods can well increase the quality factor of the BSW resonance [31] and thus make the resonant peak of the GBR thinner. In Fig. 5, the FWHMs of the Fano resonances are greatly reduced with the increase of the number of PhC periods. By further increasing the PhC periods, Fano resonance with lower sideband and higher-quality factors can also be expected. The probing signal will then be more distinguishable. However, the sidebands in the three cases are sufficiently low and the detection of the resonance with narrower FWHM

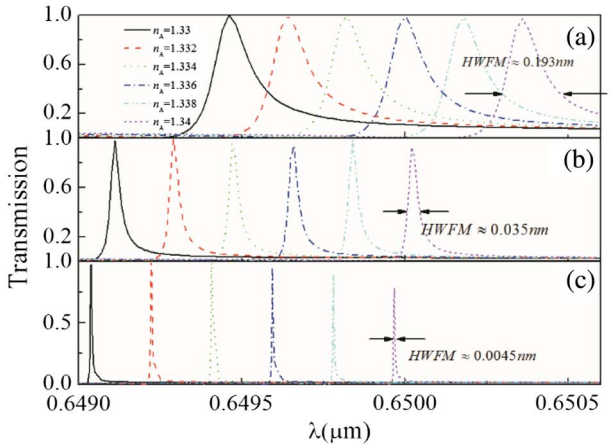

Fig. 5. Spectrum shifts when there are small variations in the refractive index of the bio-solution for GBR structure with the number of the periods of the PhC being, respectively, (a) $N = 3$, (b) $N = 4$, and (c) $N = 5$. The filling factor and the thickness of the grating are slightly modulated: (a) $f = 0.4$, $d_G = 230$ nm; (b) $f = 0.34$, $d_G = 200$ nm; (c) $f = 0.38$, $d_G = 180$ nm. The thickness of the buffer layer is fixed to dB = 320 nm.

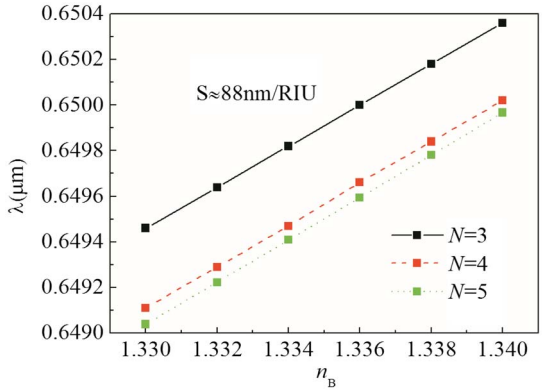

Fig. 6. GBR spectrum shift with the refractive index of the bio-solution varies from 1.33 to 1.34. The three lines represent, respectively, the three cases studied in Fig. 5.

than that of resonances in Fig. 5(c) is challenging for current spectrometers.

In Fig. 5, one can clearly find that, when the refractive index of the bio-solution changes evenly from 1.33 to 1.34, the peaks of the Fano resonances experience redshifts in all three cases. The evolving of the resonance peaks in the three cases is studied in Fig. 6. The parallel lines demonstrate that there is a ubiquitous sensitivity for all three cases, which is the same as the conclusion in the case of BSW sensors [16]. Although the sensitivity of 88 nm RIU^{-1} is in the same order but somewhat smaller than that of the SPP biosensors, the GBR biosensors perform better than the SPP counterpart regarding the concept of FOM. Even in the case of Fig. 5(a) where the number of the PhC is as small as 3, the 0.193 nm FWHM of the GBR at the incident wavelength of 650 nm leads to an FOM as large as 456. Such an FOM is four times larger than the theoretical upper limits (FOM = 108) [22] for standard gold SPP sensor and almost as large as three times the recording high FOM of the biosensors based on plasmonic nano-hole arrays [21]. The sensitivity and the FOM of the GBR biosensor are larger than that of the GMR sensor by simple grating structure or grating-on-guiding-layer configuration [13,26]. Especially, compared with the case of the grating-on-guiding-layer GMR biosensors, the stronger overlap between the resonant mode and the bio-solution in the GBR case should account for the larger sensitivity. Furthermore, when the number of the PhC increases to five [Fig. 5(c)], the FWHMs of the resonances are almost 40 times narrower than those in the case of the GBR with a three-period PhC [Fig. 5(a)], and the FOM is even in the order of 10^4.

4. SUMMARY AND CONCLUSION

The guided Bloch surface wave resonance (GBR) configuration and its sensing application are, to our knowledge, first demonstrated. By the pure dielectric hetero-structure made of a sub-wavelength grating and a 1D photonic crystal (PhC) with a few periods ($N < 5$), high-quality Fano resonances with low sidebands are realized. Due to the strong overlap between the BSW mode and the substrate bio-solution, the resonance of the BSW and thus the Fano transmission are sensitive to the refractive index modulations of the bio-solution. The high sensitivity

and large quality factor of the Fano resonance result to the large FOM for the GBR biosensors. The FOMs of the GBR biosensors are shown to be much higher than that of those biosensors, based either on GMR or on SPP configurations. At the same time, the resonance of the Bloch surface wave at the interface between the 1D PhC and the bio-solution features multi-degree of design freedoms. In the current paper, it is designed such that the normal wave vector component of the first-order diffraction in the low refractive index layer is set to be near zero. The small normal wave vector then provides the possibility of adjusting the propagation of the zeroth and the first-order diffraction independently. We thus simultaneously excite the BSW at the PhC–solution interface by the first-order diffraction and set the zeroth-order diffraction near the center of the PhC bandgap. The background transmission near the Fano transmission peak is then greatly suppressed. The lower sideband undoubtedly increases the detection limit in the sensor application. Even when large material absorption is introduced to the bio-solution, the well-suppressed transmission near the resonance peak ensures that the transmission peak is clearly distinguishable. Last but not least, it is important that, differing from the biosensor design based on SPP resonance, there is no strict refractive index limit for the dielectric composite used in the GBR. By scaling the thickness of the composing dielectrics layers properly, the sensor configuration can well be realized in any wavelength range.

In conclusion, we provide the fundamental scheme of high-quality resonance with low background transmission by the guided Bloch surface wave resonance configuration. The structure is shown to feature the advantages of both guided-mode resonance and Bloch surface wave in the realizing of label-free optical biosensing. The sensitivity of the biosensors is shown to be slightly smaller than that of the biosensor relying on SPP resonance but larger than that of guided mode resonance biosensors. At the same time, the quality factors of the guided Bloch surface wave resonances involving few-period (less than five) PhCs are shown to be sufficiently large for the detection ability of current spectrometers, and biosensors with large figures of merit are then realized by the compact guided Bloch surface wave resonance configurations. When other auxiliary means such as porous or fluorescent dielectric composites are used, we believe that GBR biosensors with better performance can be expected.

Funding. National Natural Science Foundation of China (NSFC) (11174222, 11304078, 11404102).

REFERENCES

1. J. Homola, *Surface Plasmon Resonance Based Sensors* (Springer, 2006).
2. F. Michelotti, A. Sinibaldi, P. Munzert, N. Danz, and E. Descrovi, "Probing losses of dielectric multilayers by means of Bloch surface waves," Opt. Lett. **38**, 616–618 (2013).
3. D. Yang, H. Tian, and Y. Ji, "High-Q and high-sensitivity width-modulated photonic crystal single nanobeam air-mode cavity for refractive index sensing," Appl. Opt. **54**, 1–5 (2015).
4. A. Sinibaldi, A. Fieramosca, R. Rizzo, A. Anopchenko, N. Danz, P. Munzert, C. Magistris, C. Barolo, and F. Michelotti, "Combining label-free and fluorescence operation of Bloch surface wave optical sensors," Opt. Lett. **39**, 2947–2950 (2014).
5. H. Qiao, A. H. Soeriyadi, B. Guan, P. J. Reece, and J. J. Gooding, "The analytical performance of a porous silicon Bloch surface wave-biosensors as protease biosensor," Sens. Actuators B **211**, 469–475 (2015).
6. H. Raether, *Surface Plasmons on Smooth and Rough Surfaces and on Gratings* (Springer, 1988).
7. J. Homola, "Present and future of surface plasmon resonance biosensors," Anal. Bioanal. Chem. **377**, 528–539 (2003).
8. D. R. Shankaran, K. V. Gobi, and N. Miura, "Recent advancements in surface plasmon resonance immunosensors for detection of small molecules of biomedical, food and environmental interest," Sens. Actuators B **121**, 158–177 (2007).
9. K.-L. Lee, J.-B. Huang, J.-W. Chang, S.-H. Wu, and P.-K. Wei, "Ultrasensitive Biosensors using enhanced Fano resonances in capped gold nanoslit arrays," Sci. Rep. **5**, 8547 (2015).
10. H. Zhang, Z. Jia, X. Lv, J. Zhou, L. Chen, R. Liu, and J. Ma, "Porous silicon optical microcavity biosensor on silicon-on-insulator wafer for sensitive DNA detection," Biosens. Bioelectron. **44**, 89–94 (2013).
11. S. S. Wang, R. Magnusson, J. S. Bagby, and M. G. Moharam, "Guided-mode resonances in planar dielectric-layer diffraction gratings," J. Opt. Soc. Am. A **7**, 1470–1474 (1990).
12. R. Magnusson and S. S. Wang, "New principle for optical filters," Appl. Phys. Lett. **61**, 1022–1024 (1992).
13. Y.-F. Ku, H.-Y. Li, W.-H. Hsieh, L.-K. Chau, and G.-E. Chang, "Enhanced sensitivity in injection-molded guided-mode-resonance sensors via low-index cavity layers," Opt. Express **23**, 14850 (2015).
14. M. Shinn and W. M. Robertson, "Surface plasmon-like sensor based on surface electromagnetic waves in a photonic band-gap material," Sens. Actuators B **105**, 360–364 (2005).
15. F. Giorgis, E. Descrovi, C. Summonte, L. Dominici, and F. Michelotti, "Experimental determination of the sensitivity of Bloch surface waves based sensors," Opt. Express **18**, 8087–8093 (2010).
16. R. Rizzo, N. Danz, F. Michelotti, E. Maillart, A. Anopchenko, and C. Waechter, "Optimization of angularly resolved Bloch surface wave biosensors," Opt. Express **22**, 23202–23214 (2014).
17. A. Sinibaldi, R. Rizzo, G. Figliozzi, E. Descrovi, N. Danz, P. Munzert, A. Anopchenko, and F. Michelotti, "A full ellipsometric approach to optical sensing with Bloch surface waves on photonic crystals," Opt. Express **21**, 23331–23344 (2013).
18. Y. Li, T. Yang, Z. Pang, G. Du, S. Song, and S. Han, "Phase-sensitive Bloch surface wave sensor based on variable angle spectroscopic ellipsometry," Opt. Express **22**, 21403–21410 (2014).
19. A. Sinibaldi, N. Danz, A. Anopchenko, P. Munzert, S. Schmieder, R. Chandrawati, R. Rizzo, S. Rana, F. Sonntag, A. Occhicone, L. Napione, S. D. Panfilis, M. M. Stevens, and F. Michelotti, "Label-free detection of tumor angiogenesis biomarker angiopoietin 2 using Bloch surface waves one dimensional photonic crystals," J. Lightwave Technol. **33**, 3385–3393 (2015).
20. A. Sinibaldi, N. Danz, E. Descrovi, P. Munzert, U. Schulz, F. Sonntag, L. Dominici, and F. Michelotti, "Direct comparison of the performance of Bloch surface wave and surface plasmon polariton sensors," Sens. Actuators B **174**, 292–298 (2012).
21. A. A. Yanik, A. E. Cetin, M. Huang, A. Artar, S. H. Mousavi, A. Khanikaev, J. H. Connor, G. Shvets, and H. Altug, "Seeing protein monolayers with naked eye through plasmonic Fano resonances," Proc. Natl. Acad. Sci. USA **108**, 11784–11789 (2011).
22. W. Li, X. Jiang, J. Xue, Z. Zhou, and J. Zhou, "Antibody modified gold nano-mushroom arrays for rapid detection of alpha-fetoprotein," Biosens. Bioelectron. **68**, 468–474 (2015).
23. K. S. Phillips and J. Homola, "Surface plasmon resonance-based sensors," Anal. Bioanal. Chem. **390**, 1221–1222 (2008).
24. M. Piliarik and J. Homola, "Surface plasmon resonance (SPR) sensors: approaching their limits?" Opt. Express **17**, 16505–16517 (2009).
25. J. Becker, A. Trugler, A. Jakab, U. Hohenester, and C. Sonnichsen, "The optimal aspect ratio of gold nanorods for plasmonic biosensing," Plasmonics **5**, 161–167 (2010).
26. J. D. Ryckman, M. Liscidini, J. E. Sipe, and S. M. Weiss, "Porous 1silicon structures for low-cost diffraction-based biosensing," Appl. Phys. Lett. **96**, 171103 (2010).

27. S. A. J. Moghaddas, M. Shahabadi, and M. M. Taheri, "Guided mode resonance sensor with enhanced surface sensitivity using coupled cross-stacked gratings," IEEE Sensors J. **14**, 1216–1222 (2014).
28. P. G. Hermannsson, K. T. Strensen, C. Vannahme, C. L. Smith, J. J. Klein, M.-M. Russew, G. Grützner, and A. Kristensen, "All-polymer photonic crystal slab sensor," Opt. Express **23**, 16529–16539 (2015).
29. A. E. Miroshnichenko, S. Flach, and Y. S. Kivshar, "Fano resonances in nanoscale structures," Rev. Mod. Phys. **82**, 2257–2298 (2010).
30. P. Sheng, R. S. Stepleman, and P. N. Sanda, "Exact eigenfunctions for square-wave gratings: application to diffraction and surface-plasmon calculations," Phys. Rev. B **26**, 2907–2916 (1982).
31. S. Tibuleac and R. Magnusson, "Narrow-linewidth bandpass filters with diffractive thin-film layers," Opt. Lett. **26**, 584–586 (2001).
32. X. Kang, W. Tan, Z. Wang, and H. Chen, "Optic Tamm states: the Bloch-wave-expansion method," Phys. Rev. A **79**, 043832 (2009).
33. M. G. Moharam and T. K. Gaylord, "Rigorous coupled-wave analysis of planar-grating diffraction," J. Opt. Soc. Am. **71**, 811–818 (1981).